CrystEngComm

Accepted Manuscript

ROYAL SOCIETY OF CHEMISTRY

www.rsc.org/crystengcomm

CrystEngComm

COMMUNICATION

Morphology and composition evolutions of one-dimensional $In_xAl_{1-x}N$ nanostructures induced by vapour pressure ratio

Received 00th January 20xx,
Accepted 00th January 20xx

DOI: 10.1039/x0xx00000x

www.rsc.org/

Lingyu Du, Qiang Wu,* Xiaozhu Pei, Tao Sun, Yongliang Zhang, Lijun Yang, Xizhang Wang and Zheng Hu

One-dimensional alloyed $In_xAl_{1-x}N$ nanostructures are successfully synthesized through chemical reaction of $InCl_3$, $AlCl_3$ and NH_3. By tuning the vapour pressure ratio of $InCl_3$ to $AlCl_3$, their morphologies evolve from nanocones, to nanocolumns, nanobrushes, and back to nanocones, with composition regulation in the range of $0 < x < 5$ at%.

Introduction

One-dimensional (1D) semiconductor nanomaterials have been studied intensively for years owing to the novel optical and electronic properties that depend on their bandgaps.[1,2] Polynary alloyed semiconductors can exhibit progressive evolutions of bandgaps and properties by tuning their compositions, showing great promise in various applications.[3-10] Hence, the synthesis and composition regulation of 1D nanomaterials for alloyed semiconductors are of scientific and practical significance.

For group III nitrides, the direct bandgap can be adjusted from 6.2 eV for AlN, through 3.4 eV for GaN, to 0.7 eV for InN,[11] which makes the 1D nanostructures of group III nitrides highly potential in advanced nano- and opto-electronic devices.[12-20] Various morphologies of binary nitrides (AlN, GaN, InN) have been fabricated by numerous methods, however the synthesis of alloyed nitrides with 1D geometries is highly challenging because phase separation usually happens owing to the large lattice mismatch between the two corresponding binary nitrides. Very recently, 1D nanostructures of ternary InGaN and AlGaN have been synthesized with continuously regulated compositions in the entire range, which exhibit tunable optical and electronic properties accordingly.[21-23] In contrast, most studies for ternary InAlN are focused on thin films because they can be easily prepared by diverse techniques such as vapour phase epitaxy, metal organic chemical vapour deposition and magnetron sputtering.[24-27] So far, the synthesis of 1D InAlN nanostructures is rarely reported and expensive equipment with ultrahigh vacuum is usually needed,[28-30] which highly restricts the subsequent research. Previously, we reported a convenient chloride-sourced chemical vapour deposition (CCVD) growth of alloyed $Al_xGa_{1-x}N$ nanocones over the entire composition range,[23] and the key is to match the partial pressures of Al- and Ga-containing sources during synthesis for restraining the spontaneous tendency of phase separation in the product. In this study, we have successfully extended this route to the growth of 1D InAlN nanostructures at atmospheric pressure with conventional tubular furnace. By changing the vapour pressure ratio of $InCl_3$ to $AlCl_3$, the morphology of $In_xAl_{1-x}N$ nanostructures evolve from nanocones, to nanocolumns, to 'nanobrushes', and finally back to nanocones along with the composition (x) regulation in the range of $0 < x < 5$ at%. The results also indicate that the In content of the ternary $In_xAl_{1-x}N$ nanostructures is limited by using this CCVD method.

Experimental

The growth of 1D $In_xAl_{1-x}N$ nanostructures was conducted in a three-temperature-zone tubular furnace (Fig. S1, ESI†) by using $AlCl_3$, $InCl_3$ and NH_3 as Al, In and N sources, respectively. Typically, $AlCl_3$, $InCl_3$ and a Si (100) substrate were placed separately at the three zones along the gas flow direction. After the system was evacuated and flushed with Ar gas for several times, the three zones were heated to appropriate temperatures under the protection of Ar gas. The vaporization temperature for $AlCl_3$ is set at 130 °C owing to the fact that higher $AlCl_3$ vapour pressure would result in the formation of large AlN particles.[13] The $InCl_3$ source was heated in the range of 300-500 °C to adjust the vapour pressure ratio of $InCl_3$ to $AlCl_3$. The deposition temperature of the products was set at 700 °C. When the three zones were heated to the set temperatures, 300 mL min^{-1} of Ar was introduced for transporting the $AlCl_3$ and $InCl_3$ vapours downstream to the Si (100) substrate, and 30 mL min^{-1} of NH_3 was imported behind the place of $InCl_3$ powder (Fig. S1, ESI†). The growth was lasted for 2 h and then the system was cooled under the protection of Ar.

Key Laboratory of Mesoscopic Chemistry of MOE and Collaborative Innovation Center of Chemistry for Life Sciences, Jiangsu Provincial Laboratory for Nanotechnology, School of Chemistry and Chemical Engineering, Nanjing University, Nanjing 210023, China.

E-mail: wqchem@nju.edu.cn

†Electronic Supplementary Information (ESI) available: Schematic illustration of tubular furnace, additional TEM and SEM images. See DOI: 10.1039/x0xx00000x

The morphologies of the products were examined by scanning electron microscopy (SEM, Hitachi S-4800) equipped with an energy dispersive X-ray spectroscopy (EDS) detector and high resolution transmission electron microscopy (HRTEM, JEOL-2100). The structures of the products were characterized by X-ray diffraction (XRD, Bruker X-ray diffractometer, D8 Advance A25, Co target, $\lambda_{K\alpha1}$ = 0.178897 nm). The optical properties were investigated by Raman spectrometer (Horiba, LabRAM Aramis, excited with an Ar^+ line at 532 nm) and photoluminescence spectroscopy (Hitachi F-7000, excited with a Xe lamp at 290 nm) at room temperature.

Results and discussion

The morphologies of the $In_xAl_{1-x}N$ products evolve from nanocones to nanocolumns, 'nanobrushes', and back to nanocones with increasing the vaporization temperature (T_{vap}) of $InCl_3$, as shown in Fig. 1. Specifically, the product presents as quasi-aligned nanocone array on the Si substrate at the T_{vap} of 330 °C or lower (Fig. S2, ESI†). As exemplified by the product at 300 °C, the nanocones possess the diameters of ~100 nm on the roots and ~10 nm on the tips (Fig. 1a,b, Fig. S3, ESI†), very similar to the pure AlN nanocones formed in the absence of $InCl_3$.[31-33] Increasing the T_{vap} of $InCl_3$ to 350 °C results in a marked morphology change from nanocones to nanocolumns. The nanocolumns have hexagonal cross sections with the diameter of 100~200 nm and the length of 5-6 μm (Fig. 1c,d). Further elevation of the T_{vap} to 380 °C shows negligible influence on the nanocolumn morphology except for an obvious increase in the diameter (Fig. 1e,f). TEM observation on the nanocolumns scraped from the Si substrate reveals that their diameters are 200~400 nm, and the interplanar distance of 0.253 nm can be assigned to the (002) planes (Fig. 2a). As the T_{vap} of $InCl_3$ is set at 400 °C, nanocone bundles are grow epitaxially on the nanocolumns, forming the heterostructures of 'nanobrushes', quite like the Chinese brushes. The nanocolumns have the diameter of 200~400 nm and the length of the nanocones is 500~1000 nm (Fig. 1g,h). Such a morphology can remain till to the T_{vap} of 450 °C (Fig. 1i,j). As depicted in Fig. 2b, the 'nanobrushes' consist of solid rodlike roots and disjugate tips of conelike bundles. These nanocones grow along the [001] direction with the interplanar spacing (0.241 nm) for (101) planes. Surprisingly, the morphology of the product turns back to the nanocones when the T_{vap} of $InCl_3$ is increased to be 460 °C or higher, e.g., 500 °C (Fig. 1k,l, Fig. S2 in ESI†). The morphological evolution reflects the great influence of the $InCl_3$ vapour pressure on the $In_xAl_{1-x}N$ products.

The crystalline structure of the $In_xAl_{1-x}N$ nanomaterials is characterized by XRD. As shown in Fig. 3a, only one diffraction peak is presented which corresponds to (002) planes by comparing the XRD pattern of pure AlN sample. The absence of other diffractions indicates that these nanostructures are preferentially grown along the [001] direction, in consistence with the HRTEM results. All of the (002) peaks are singlet and shift to the lower angle side in comparison with that of pure AlN, which indicates that In atoms with large radii are uniformly incorporated into the AlN lattice to form alloyed $In_xAl_{1-x}N$. More interestingly, the shift of the (002) peaks is first toward the lower angle side and then back to higher angle side with increasing the T_{vap} of $InCl_3$. According to the diffraction angles

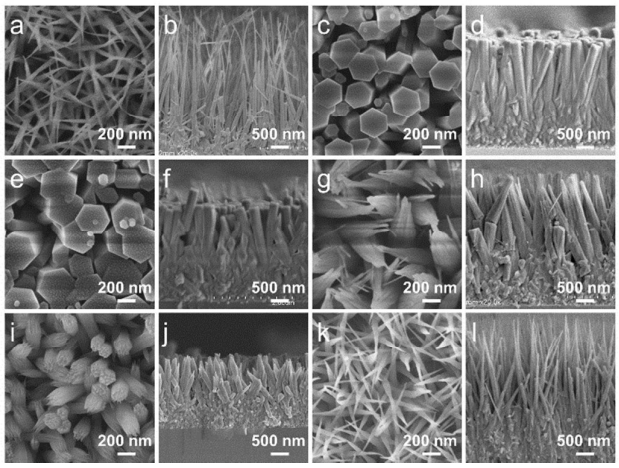

Fig. 1 Morphology evolution of $In_xAl_{1-x}N$ nanostructures with the T_{vap} of $InCl_3$. (a, b) 300°C , (c, d) 350 °C, (e, f) 380 °C , (g, h) 400 °C (i,j) 450 °C, (k, l) 500 °C .

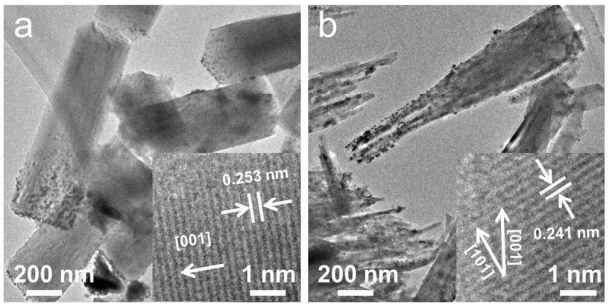

Fig. 2 Typical TEM and HRTEM images of the $In_xAl_{1-x}N$ nanomaterials obtained at the T_{vap} of 380 °C (a) and 400 °C (b). Note: The interplanar distances of 0.253 nm (inset of a) and 0.241 nm (inset of b) correspond to (002) and (101) planes respectively.

of the serial $In_xAl_{1-x}N$ products, the In contents are calculated by the Vegard's law,[34] which show a volcano-shape change tendency as depicted in Fig. 3b. This is very similar to the change of the In contents measured by the EDS, within the error range. The composition evolution of the serial $In_xAl_{1-x}N$ products is also reflected by the Raman spectra (Fig. 3c), in which the E_2(high) mode exhibits a similar shift tendency. In addition, the element distributions of Al and In are uniform along the axial direction of these 1D nanostructures (Fig. S4, ESI†), in consistence with the XRD results. The preceding results indicate that 1D alloyed $In_xAl_{1-x}N$ nanostructures have been successfully synthesized at 700 °C by the convenient CCVD method, and the In content can be regulated in the range of $0 < x < 5.0$ at% with the highest In content for the $In_xAl_{1-x}N$ nanocolumn arrays obtained at the T_{vap} of 380 °C for $InCl_3$. By decreasing the deposition temperature, the In content in the $In_xAl_{1-x}N$ products can be increased a little but with a poor morphologic unicity (Fig. S5, ESI†). Hence, the deposition temperature of 700 °C is preferred.

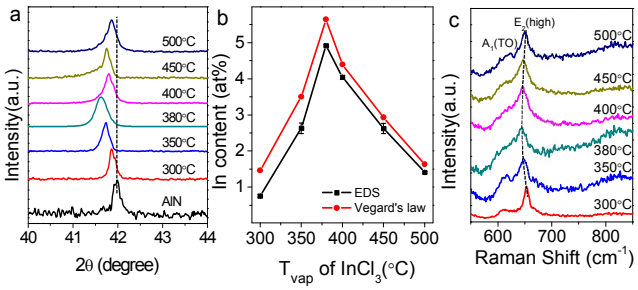

Fig. 3 XRD patterns (a), In contents (b) and Raman spectra (c) of the $In_xAl_{1-x}N$ samples prepared at different T_{vap} of $InCl_3$. XRD pattern for pure AlN nanocones is also shown in (a) for comparison. Note: The error bar in the EDS curve (b) is the standard deviation based on three detected spots.

The morphology and composition evolutions of the 1D alloyed $In_xAl_{1-x}N$ nanostructures are well correlated with the vapour pressure ratio of $InCl_3$ to $AlCl_3$ as shown in Fig. 4. It is generally accepted that the morphology of the CVD-grown materials is closely related to the supersaturation degree during the synthesis.[1] Particularly, to prepare alloyed group III nitrides, it is necessary to achieve the matchable partial pressures of the respective precursors for restraining the spontaneous tendency of the phase separation.[23] This indicates the partial pressures of the precursors play a dominant role in controlling the morphology and composition of semiconductor nanostructures. As known, the partial pressure of a substance is dependent on the T_{vap}. In this study, the T_{vap} for $AlCl_3$ is fixed while that for $InCl_3$ is varied, therefore, the partial pressure ratio of $InCl_3$ to $AlCl_3$, i.e. $p(InCl_3)/p(AlCl_3)$ (also referred to as R), can be increased simply by elevating the T_{vap} of $InCl_3$. As shown in Fig. 4, the plot of logR versus T_{vap} of $InCl_3$ presents a quasi-linear relationship. Combining the evolution of the products (Fig. 1 and 3), it is learnt that the R is critical for the morphology of 1D alloyed $In_xAl_{1-x}N$ nanostructures. Specifically, the product presents the morphology of hexagonal nanocolumns at the R of 10^{-2}~0.3, and of 'nanobrushes' at the R of 0.3~3, while shows the nanocone geometry at the R below 10^{-2} or above 3, similar to the case without $InCl_3$.

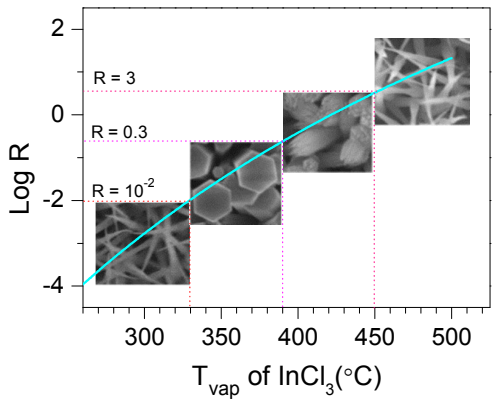

Fig. 4 Relationship between the morphologies and the vapour pressure ratio of $InCl_3$ to $AlCl_3$. The blue curve is the plot of LogR versus T_{vap} of $InCl_3$.

The influence of $InCl_3$ vapour could be understood as follows. In the absence of $InCl_3$, the chemical reaction between $AlCl_3$ and NH_3 yields AlN nanocones along the preferential growth direction of [001].[31] The introduction of $InCl_3$ into the growth leads to the formation of 1D $In_xAl_{1-x}N$ nanomaterials by incorporating In atoms into the AlN lattice. At the R below 10^{-2}, the vapour pressure of $InCl_3$ is not high enough to affect the growth habit of AlN crystal, hence the nanocone morphology is remained. With a higher vapour pressure of $InCl_3$, more In-containing species are involved in the growth, which enhance the growth rate of [100] direction while suppress that of [001], thus the product morphology changes from nanocones to nanocolumns with smaller length (Fig. 1b,d). When the R is in the range of $0.3 < R < 3$, InAlN 'nanobrushes' are formed. It should be noted that the elevation of furnace temperature has a little bit delay in our synthesis, hence at the initial growth stage the T_{vap} of $InCl_3$ is lower than the set value, resulting in a smaller vapour pressure of $InCl_3$, and thus forming nanocolumns as the case of $10^{-2} < R < 0.3$. As the temperature of the second zone reaches the desired value, the vapour pressure of $InCl_3$ is increased accordingly, and the InAlN nanomaterials with high In content are expected. However, it is well known that InN has a poor stability at high temperature (> 500 °C),[35] and the increase of In content in the ternary InAlN could deteriorate its stability. In this case, the high vapour pressure of $InCl_3$ brings about more and more InN species. At the growth temperature of 700 °C, partial InN are decomposed into In nanoparticles attaching on the products (Fig. S6, ESI†), and thus the In species for alloying is decreased, which leading to the formation of nanocones. Hence the brush-like heterostructures are obtained. As the R is higher than 3, the vapour pressure of $InCl_3$ is largely increased owing to the high vaporization temperature. However, such temperature directly enables the reaction between $InCl_3$ and NH_3 during the vapour transferring period,[36] which much decreases the $InCl_3$ concentration near the Si substrate, and hence the InAlN nanocones are formed, quite similar to the case for T_{vap} of $InCl_3$ below 330 °C.

From above discussion, it is learnt that the 1D alloyed InAlN nanostructures can be synthesized by the CCVD method, however the In content is limited in the range of 0~5 at% owing to the difficulties in the supplying of In source and the instability of InAlN with high In content. This suggests that a low-temperature growth method should be adopted for further increasing the In content.

The InAlN nanostructures with typical morphologies of nanocolumns, 'nanobrushes' and nanocones exhibit promising optical properties. As shown in Fig. 5, emission bands centred at ~470 nm are observed for the three InAlN samples. In comparison with the pure AlN nanocones, the emissions of the InAlN samples broaden with slight red-shifts and much enhanced intensities. The blue emission could be ascribed to the nitrogen vacancy and the unavoidable oxygen impurity in InAlN.[31] The detailed mechanism of the blue emission still needs further investigation. It is shown that the emission bands of different InAlN samples show negligible shift owing to the small variation of In content. However, the emission intensities decrease with increasing the T_{vap} of $InCl_3$ from 350 °C to

500 °C. This is possibly owing to the morphology of the nanostructure arrays on the Si substrate.[37] Specifically, the nanocolumns (350 °C) have larger top-planar area than the nanobrushes (400 °C) and nanocones (500 °C), which result in the stronger emission owing to the more nitrogen vacancies and oxygen impurities. These 1D InAlN nanostructures show great potential in the nanoscale optoelectronic devices in compared with the 0D or 2D InAlN materials.[38]

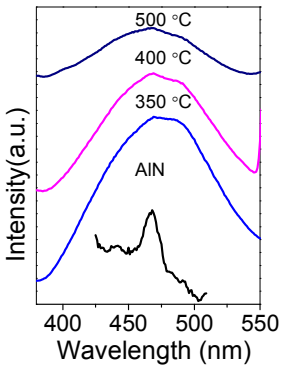

Fig. 5 Photoluminescence spectra for the InAlN samples with three typical morphologies and pure AlN nanocones.

Conclusions

We report the successful preparation of 1D alloyed $In_xAl_{1-x}N$ nanostructures via a convenient CCVD method. By increasing the vaporization temperature of $InCl_3$, the morphology of $In_xAl_{1-x}N$ nanostructures evolves from nanocones, to nanocolumns, to 'nanobrushes', and back to nanocones, and their composition (x) is tuned in the range of $0 < x < 5$ at%, showing a volcano-shape change tendency. The morphology and composition evolutions are well correlated with the vapour pressure ratio of $InCl_3$ to $AlCl_3$. The 1D $In_xAl_{1-x}N$ nanostructures show blue luminescence properties, suggesting potential applications in light emitting diodes. The results also indicate that the In content of the ternary $In_xAl_{1-x}N$ nanostructures is limited by using this chloride-sourced chemical vapour deposition method, and low-temperature route is suggested for further increasing the In content.

Acknowledgements

This work was jointly supported by the Natural Science Foundation of China (21173115, 21373108 and 21473089) and the National Basic Research Program of China (2013CB932902).

Notes and references

1 Y. N. Xia, P. D. Yang, Y. G. Sun, Y. Y. Wu, B. Mayers, B. Gates, Y. D. Yin, F. Kim and H. Q. Yan, *Adv. Mater.*, 2003, **15**, 353–389.
2 N. P. Dasgupta, J. W. Sun, C. Liu, S. Brittman, S. C. Andrews, J. Lim, H. W. Gao, R. X. Yan and P. D. Yang, *Adv. Mater.*, 2014, **26**, 2137–2184.
3 Y. L. Zhang, J. Cai, T. P. Ji, Q. Wu, Y. Y. Xu, X. Z. Wang, T. Sun, L. J. Yang and Z. Hu, *Nano Res.*, 2015, **8**, 584–591.
4 C. S. Jung, H. S. Kim, G. B. Jung, K. J. Gong, Y. J. Cho, S. Y. Jang, C. H. Kim, C. W. Lee and J. Park, *J. Phys. Chem. C,* 2011, **115**, 7843–7850.
5 A. Pan, H. Yang, R. B. Liu, R. C. Yu, B. S. Zou and Z. L. Wang, *J. Am. Chem. Soc.*, 2005, **127**, 15692–15693.
6 K. Tomioka, J. Motohisa, S. Hara, K. Hiruma and T. Fukui, *Nano Lett.*, 2010, **10**, 1639–1644.
7 G. R. Shao, G. H. Chen, J. Zuo, M. Gong and Q. Yang, *Langmuir*, 2014, **30**, 7811–7822.
8 X. N. Wang, Y. Xu, R. Tong, X. L. Zhou, Q. Li and H. Wang, *CrystEngComm*, 2015, **17**, 960-966.
9 F. J. Xu, B. Xue, F. D. Wang and A. G. Dong, *Chem. Mater.*, 2015, **27**, 1140–1146.
10 Y. J. Zhang, L. Li, D. L. Li and Q. B. Wang, *J. Phys. Chem. C*, 2015, **119**, 1496–1499.
11 J. Wu, W. Walukiewicz, K. M. Yu, J. W. Ager III, S. X. Li, E. E. Haller, H. Lu and W. J. Schaff, *Solid State Commun.*, 2003, **127**, 411–414.
12 J. Zheng, Y. Yang, B. Yu, X. B. Song and X. G. Li, *ACS Nano*, 2008, **2**, 134–142.
13 F. Zhang, Q. Wu, X. B. Wang, N. Liu, J. Yang, Y. M. Hu, L. S. Yu, X. Z. Wang, Z. Hu and J. M. Zhu, *J. Phys. Chem. C*, 2009, **113**, 4053–4058.
14 C. Y. He, X. Z. Wang, Q. Wu, Z. Hu, Y. W. Ma, J. J. Fu and Y. Chen, *J. Am. Chem. Soc.*, 2010, **132**, 4843-4847.
15 F. Yuan, B. D. Liu, Z. E. Wang, B. Yang, Y. Yin, B. Dierre, T. Sekiguchi, G. F. Zhang and X. Jiang, *ACS Appl. Mater. Interfaces*, 2013, **5**, 12066–12072.
16 M. I. den Hertog, F. González-Posada, R. Songmuang, J. L. Rouviere, T. Fournier, B. Fernandez and E. Monroy, *Nano Lett.*, 2012, **12**, 5691–5696.
17 M. D. Brubaker, P. T. Blanchard, J. B. Schlager, A. W. Sanders, A. Roshko, S. M. Duff, J. M. Gray, V. M. Bright, N. A. Sanford and K. A. Bertness. *Nano Lett.*, 2013, **13**, 374–377.
18 X. Zhou, M. Y. Lu, Y. J. Lu, E. J. Jones, S. Gwo and S. Gradecak, *ACS Nano*, 2015, **9**, 2868–2875.
19 X. B. Wang, J. H. Song, F. Zhang, C. Y. He, Z. Hu and Z. L. Wang, *Adv. Mater.*, 2010, **22**, 2155-2158.
20 H. Q. Liu, S. Chu, R. F. Peng, M. Liu, Z. X. Chen, B. Jin and S. J. Chu, *CrystEngComm*, 2015, **17**, 4818-4824.
21 T. Kuykendall, P. Ulrich, S. Aloni and P. D. Yang, *Nat. Mater.*, 2007, **6**, 951–956.
22 C. Hahn, Z. Y. Zhang, A. Fu, C. H. Wu, Y. J. Hwang, D. J. Gargas and P. D. Yang, *ACS Nano*, 2011, **5**, 3970–3976.
23 C. Y. He, Q. Wu, X. Z. Wang, Y. L. Zhang, L. J. Yang, N. Liu, Y. Zhao, Y. N. Lu and Z. Hu, *ACS Nano*, 2011, **5**, 1291–1296.
24 C. Hums, J. Bläsing, A. Dadgar, A. Diez, T. Hempel, J. Christen, A. Krost, K. Lorenz and E. Alves, *Appl. Phys. Lett.*, 2007, **90**, 022105.
25 J. M. Mánuel, F. M. Morales, J. G. Lozano, D. González, R. García, T. Lim, L. Kirste, R. Aidam and O. Ambacher, *Acta Mater.*, 2010, **58**, 4120–4125.
26 R. B. Chung, F. Wua, R. Shivaraman, S. Keller, S. P. DenBaars, J. S. Speck and S. Nakamura, *J. Cryst. Growth*, 2011, **324**, 163–167.
27 Q. F. Han, C. H. Duan, G. P. Du, W. Z. Shi and L. C. Ji, *J. Electron. Mater.*, 2010, **39**, 489–493.
28 J. Kamimura, T. Kouno, S. Ishizawa, A. Kikuchi and K. Kishino, *J. Cryst. Growth*, 2007, **300**, 160–163.
29 E. A. Serban, P. O. Å. Persson, I. Poenaru, M. Junaid, L. Hultman, J. Birch and C. L. Hsiao, *Nanotechnology*, 2015, **26**, 215602.
30 C. L. Hsiao, R. Magnusson, J. Palisaitis, P. Sandström, P. O. Å. Persson, S. Valyukh, L. Hultman, K. Järrendahl and J. Birch, *Nano Lett.*, 2015, **15**, 294–300.

31 C. Liu, Z. Hu, Q. Wu, X. Z. Wang, Y. Chen, H. Sang, J. M. Zhu, S. Z. Deng and N. S. Xu, *J. Am. Chem. Soc.*, 2005, **127**, 1318–1322.
32 N. Liu, Q. Wu, C. Y. He, H. S. Tao, X. Z. Wang, W. Lei and Z. Hu, *ACS Appl. Mater. Interfaces*, 2009, **1**, 1927–1930.
33 W. J. Qian, Y. L. Zhang, Q. Wu, C. Y. He, Y. Zhao, X. Z. Wang and Z. Hu, *J. Phys. Chem. C*, 2011, **115**, 11461–11465.
34 L. Vegard, *Z. Phys.*, 1921, **5**, 17–26.
35 D. A. Neumayer and J. G. Ekerdt, *Chem. Mater.*, 1996, **8**, 9-25.
36 B. S. Simpkins, A. D. Kansal and P. E. Pehrsson, *Cryst. Growth Des.*, 2010, **10**, 3887–3891.
37 T. Andelman, Y. Y. Gong, M. Polking, M. Yin, I. Kuskovsky, G. Neumark and S. O'Brien, *J. Phys. Chem. B*, 2005, **109**, 14314–14318.
38 F. Qian, S. Gradečak, Y. Li, C. Y. Wen and C. M. Lieber, *Nano Lett.*, 2005, **5**, 2287–2291.

CrystEngComm

COMMUNICATION

Table of contents entry

Morphology and composition evolutions of one-dimensional $In_xAl_{1-x}N$ nanostructures induced by vapour pressure ratio

Lingyu Du, Qiang Wu,* Xiaozhu Pei, Tao Sun, Yongliang Zhang, Lijun Yang, Xizhang Wang and Zheng Hu

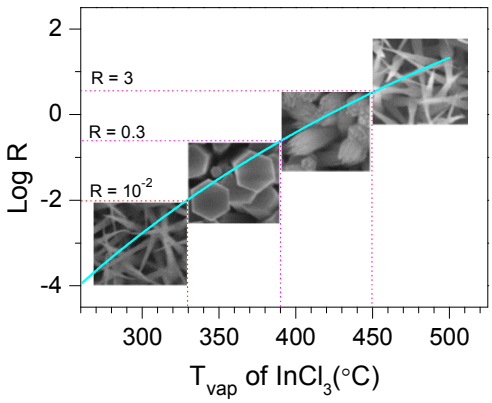

Morphology and composition of one-dimensional alloyed $In_xAl_{1-x}N$ nanostructures are regulated by tuning the vapour pressure ratio of $InCl_3$ to $AlCl_3$ during the chemical vapour desposition.